doi:10.1016/j.jmb.2008.11.025 J. Mol. Biol. (2009) 385, 1556–1567

JMB

Available online at www.sciencedirect.com

ScienceDirect

ELSEVIER

Somatostatin: A Novel Substrate and a Modulator of Insulin-Degrading Enzyme Activity

Chiara Ciaccio[1,2]†, Grazia R. Tundo[1,2]†, Giuseppe Grasso[3], Giuseppe Spoto[3,4], Daniela Marasco[5], Menotti Ruvo[5], Magda Gioia[1], Enrico Rizzarelli[3,4] and Massimo Coletta[1,2]*

[1]*Department of Experimental Medicine and Biochemical Sciences, University of Roma Tor Vergata, Via Montpellier 1, I-00133 Roma, Italy*

[2]*Interuniversity Consortium for the Research on the Chemistry of Metals in Biological Systems, P.za Umberto I 1, I-70100 Bari, Italy*

[3]*Department of Chemistry, University of Catania, V.le A. Doria, Catania, Italy*

[4]*Institute of Biostructure and Bioimaging, CNR, Catania, Italy*

[5]*Institute of Biostructure and Bioimaging CNR, Napoli, Italy*

Received 11 July 2008; received in revised form 15 October 2008; accepted 17 November 2008
Available online 25 November 2008

Edited by J. Weissman

Insulin-degrading enzyme (IDE) is an interesting pharmacological target for Alzheimer's disease (AD), since it hydrolyzes β-amyloid, producing non-neurotoxic fragments. It has also been shown that the somatostatin level reduction is a pathological feature of AD and that it regulates the neprilysin activity toward β-amyloid.

In this work, we report for the first time that IDE is able to hydrolyze somatostatin [k_{cat} (s^{-1}) = 0.38 (±0.05); K_m (M) = 7.5 (±0.9) × 10^{-6}] at the Phe6–Phe7 amino acid bond. On the other hand, somatostatin modulates IDE activity, enhancing the enzymatic cleavage of a novel fluorogenic β-amyloid through a decrease of the K_m toward this substrate, which corresponds to the 10–25 amino acid sequence of the Aβ(1–40). Circular dichroism spectroscopy and surface plasmon resonance imaging experiments show that somatostatin binding to IDE brings about a concentration-dependent structural change of the secondary and tertiary structure(s) of the enzyme, revealing two possible binding sites. The higher affinity binding site disappears upon inactivation of IDE by ethylenediaminetetraacetic acid, which chelates the catalytic Zn^{2+} ion. As a whole, these features suggest that the modulatory effect is due to an allosteric mechanism: somatostatin binding to the active site of one IDE subunit (where somatostatin is cleaved) induces an enhancement of IDE proteolytic activity toward fluorogenic β-amyloid by another subunit. Therefore, this investigation on IDE–somatostatin interaction contributes to a more exhaustive knowledge about the functional and structural aspects of IDE and its pathophysiological implications in the amyloid deposition and somatostatin homeostasis in the brain.

Keywords: insulin-degrading enzyme; kinetics; fluorogenic β-amyloid peptide; somatostatin; circular dichroism

*Corresponding author. Department of Experimental Medicine and Biochemical Sciences, University of Roma Tor Vergata, Via Montpellier 1, I-00133 Roma, Italy. E-mail address: coletta@seneca.uniroma2.it.

† C.C. and G.T. contributed equally to this work.

Abbreviations used: IDE, insulin-degrading enzyme; AD, Alzheimer's disease; TFA, trifluoroacetic acid; EDANS, 5-[(2-aminoethyl)-amino]naphthalene-1-sulfonic acid; Dabcyl-OSu, [4-((4-(dimethyl-amino) phenyl)azo)benzoic acid]-N-hydroxysuccinimide ester; Fmoc, fluorenylmethoxycarbonyl; LC, liquid chromatography; MS, mass spectrometry; AP-MALDI MS, atmospheric pressure matrix-assisted laser desorption/ionization mass spectrometry; SPRI, surface plasmon resonance imaging; EDTA, ethylenediaminetetraacetic acid; FβA, fluorogenic β-amyloid; PBS, phosphate-buffered saline; RF, radio frequency; NCE, normalized collision energy; PDMS, poly(dimethylsiloxane).

Introduction

Insulin-degrading enzyme (IDE, insulysin) is a 110-kDa zinc-metalloprotease, involved in the hydrolysis of short polypeptides that vary significantly in sequence, many of which (such as insulin, β-amyloid, amylin, glucagon, β-endorphin, and atrial natriuretic peptide) show a propensity to form under certain conditions β-sheet-rich amyloid fibrils.[1] IDE expression is ubiquitous in human tissue, being particularly abundant in the brain, liver, and muscles, where it is found primarily in the cytosol, peroxisomes, and endosomes; on the other hand, only a small fraction of the enzyme is located on the plasma membrane and in the mithocondria.[2,3] Genetic studies indicate that IDE region of chromosome 10q is associated to the late-onset Alzheimer's disease (AD) and type II diabetes; furthermore, IDE knocked-out-based work shows glucose intolerance, hyperinsulinemia, and accumulation of β-amyloid in the brain.[4] These results suggest that IDE may be involved in the pathophysiological pathways common to AD, type II diabetes, and hyperinsulinemia.[5–7]

IDE appears to be a multisubunit protein, each subunit being formed by two domains, namely, (i) the N-terminal domain (IDE-N), where the catalytic site is located, and (ii) the C-terminal domain (IDE-C). X-ray crystallography shows that the enzyme looks like a "clam with two valves", where IDE-N and IDE-C are kept together through a "latch".[8] The latch flexibility allows IDE to adopt two different conformations, the "open" and the "closed" state. Only in the open conformation are substrates and reaction products free to go in and out of the active site, favoring the enzymatic activity; on the other hand, in the closed state, the active-site accessibility is severely limited, being characterized by a low enzymatic activity.[9]

Native IDE exists as a mixture of monomer, dimer, and tetramer, which are in equilibrium according to the mass law. The dimeric form has been postulated to be the most active one,[10] although the evidence is quite indirect and not unequivocally proved. This feature might be referable to a greater propensity of the dimeric species to adopt the open conformation. Functional studies on IDE activity modulation by metabolic peptides, such as dynorphins, have suggested an allosteric mechanism, according to which the binding of a peptide to a subunit brings about an alteration of the affinity and enzymatic activity of IDE for substrates interacting with the adjacent one, likely shifting the equilibrium in favor to the open state.[1] However, it must be pointed out that the impossibility to physically separate the oligomeric forms (i.e., the monomer, the dimer, and the tetramer interconnected by the mass law equilibrium) does not allow obtaining distinct functional information on them, vanishing at this stage any attempt to extract meaningful knowledge on the potential cooperative activity of IDE, even though data reported in this article underlie some aspects of the possible intersubunit functional interaction.

IDE substrate specificity has been proposed not to depend on the amino acid sequence (even though it preferentially cleaves basic and hydrophobic amino acids), but mostly on the β-sheet structure recognition. Thus, several peptides cleaved by insulysin adopt the β-sheet conformation when they bind the enzyme, showing a structural arrangement similar to that occurring during self-association of amyloidogenic proteins. Experimental studies confirm that the same residues involved in amyloidogenic protein fibrillation are also responsible for insulysin binding.[3,11]

Somatostatin is a cyclic tetradecapeptide first isolated from the hypothalamic tissue as a hormone that inhibits the release of growth hormone.[12] However, it is now considered a multifunctional peptide, located in the central nervous system and in the gastrointestinal system,[13] where it is involved in the regulation of glucose homeostasis with insulin and glucagon. It has been reported that the somatostatinergic network modulates cognitive and sensory functions in the brain, motor activity, and sleep.[14] In addition, somatostatin level decreases with age,[15] underlying a possible role of somatostatin in the decay of cerebral activities of elder people. A role of somatostatin in the evolution of AD has also been proposed, since the lack of somatostatin in the cortex and hippocampus has been shown to be linked to an impairment of cognitive function and memory.[16] Moreover, a reduction of this neuropeptide has been observed in the cortical and cerebrospinal fluid of AD patients,[17–20] being associated to a selective degeneration of somatostatin-producing neurons[21,22] and an altered expression of all five somatostatin receptors in cortical neurons.[16] Recently, it has been shown that somatostatin regulates β-amyloid metabolism by increasing the enzymatic activity of neprilysin (which is the most important enzyme responsible for the hydrolysis of β-amyloid together with IDE) in primary cortical neurons; a modification of neprilysin localization induced by somatostatin has also been observed.[19,23,24]

Seq. βA(1-40) D-A-E-F-R-H-D-S-G-Y-E-**V-H-H-Q**-K-L-**V-F-F-A**-E-D-V-G-S-N-**K-G**-A-I-I-G-L-M-V-G-G-V-V

Seq.FβA Dabcyl-Y-E-**V-H-H-Q**-K-L-**V-F-F-A**-E-D-V-E-(Edans)-NH2

Fig. 1. Amino acid sequences of Aβ(1–40) (above) and FβA (below) are compared. Arrows indicate the cleavage sites by IDE.

Altogether, the available data suggest a possible role of both IDE and somatostatin in the pathogenesis of AD. Therefore, a characterization of somatostatin–IDE interaction and its functional effect on IDE activity should cast some light on the molecular interrelationships at the origin of the pathophysiological events of AD. In the present work, we report for the first time that somatostatin is a substrate of IDE and an allosteric modulator of IDE activity toward a novel fluorogenic β-amyloid (FβA) peptide, establishing the functional basis for a link between IDE activity and somatostatin role in the brain.

Results

Hydrolysis of FβA by IDE

FβA contains all cleavage sites (except one) of human Aβ(1–40) (Fig. 1), and the kinetics of its processing by IDE has been investigated in order to obtain the catalytic parameters that characterize the process. It is not prone to aggregation, since it has been synthesized to reduce self-assembly properties of the intact β-amyloid.

No evidence of a sigmoidal dependence of the enzymatic velocity on the substrate concentration is detectable (see Fig. S1), indicating that data do not significantly diverge from a simple enzymatic behavior. Although this feature does not rule out completely some functional interaction among different subunits, the impossibility to discriminate between monomers, dimers, and tetramers (all concurrently present in the enzyme solution under the experimental conditions investigated) does not allow extracting from these data any useful information on the interaction among subunits. Nonetheless, the linear dependence of the double reciprocal plot of velocity *versus* substrate concentration (Fig. 2) allows a phenomenological analysis of data according to the Michaelis–Menten mechanism, producing the overall catalytic parameters (Table 1). The possibility of describing satisfactorily the enzymatic activity of IDE with a single set of catalytic parameters indeed suggests either that all cleavage sites (see Fig. 1) have similar values or that there is a largely predominant cleavage site (likely that between His14 and Gln15)[25] to which the observed catalytic parameters are referable. In either case, it is important to underline that the value of K_m [=2.3 (±0.35)×10^{-5} M] is closely similar to that reported for the Aβ(1–40),[9] suggesting that IDE interacts with the FβA peptide in a fashion similar to that with the native Aβ(1–40). On the other hand, the value of k_{cat} (=62±7 s^{-1}) for the FβA peptide is much faster than what was reported for the native Aβ(1–40), indicating that the energy barrier for the bond cleavage is somehow reduced in the complex between IDE and the FβA peptide.

Table 1. Catalytic parameters for the enzymatic processing of the FβA peptide, Aβ(1–40), and somatostatin by IDE at pH7.3 and 37 °C

	k_{cat}/K_m (M^{-1} s^{-1})	k_{cat} (s^{-1})	K_m (M)
Somatostatin[a]	5.1 (±0.7)×10^4	0.38 (±0.05)	7.5 (±0.9)×10^{-6}
FβA peptide[a]	2.7 (±0.4)×10^6	62.7 (±7.1)	2.3 (±0.3)×10^{-5}
FβA peptide[a] +40 μM SsT	5.2 (±0.6)×10^6	61.0 (±6.9)	1.2 (±0.2)×10^{-5}
Aβ(1–40)[b]	3.2 (±0.4)×10^5	8.0 (±1.0)	2.5 (±0.4)×10^{-5}

[a] This work.
[b] From Ref. 9.

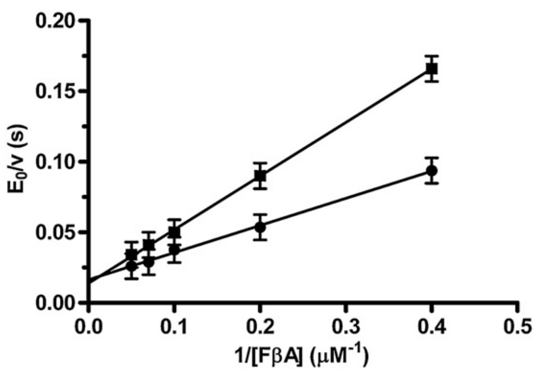

Fig. 2. Lineweaver–Burk plot of kinetic data for the hydrolysis of FβA by IDE. Increasing concentrations of FβA were incubated with 10 nM of IDE in 40 mM phosphate buffer at pH7.3 and 37 °C in the absence (■) and in the presence (●) of 40 μM somatostatin. The reaction was followed by the increase of fluorescence at 472 nm that occurred upon cleavage by the enzyme (excitation wavelength=336 nm). Continuous line was obtained by linear least-squares analysis according to the following equation:

$$\frac{[E_0]}{v} = \frac{K_m}{k_{cat}} \cdot \frac{1}{[S]} + \frac{1}{k_{cat}} \quad (3)$$

where $[E_0]$ is the total IDE concentration, v is the observed rate constant (expressed as s^{-1}), K_m is the Michaelis constant, k_{cat} is the rate constant of the rate-limiting step, and $[S]$ is the substrate concentration. Catalytic parameters are reported in Table 1.

Somatostatin hydrolysis by IDE

HPLC analysis of somatostatin in the presence of 10 nM IDE indicates that somatostatin is enzymatically processed by the IDE. Although the enzymatic processing of somatostatin has already been reported by other Zn-peptidases, such as neurolysin (EC 3.4.24.16) and thimet oligopeptidase (EC 3.4.24.15),[26,27] this is the first time that the enzymatic processing by IDE is observed, suggesting a possible influence of IDE on the homeostasis of somatostatin in the brain.

Also in the case of somatostatin hydrolysis by IDE, we do not observe any sigmoidal dependence of enzymatic kinetics on somatostatin concentration (see Fig. S2) and the same considerations can be formulated (see above). On the other hand, the enzymatic processing of somatostatin by IDE follows a Michaelis–Menten mechanism (Fig. 3), and overall catalytic parameters characterizing the single cleavage event (see below) were obtained (Table 1).

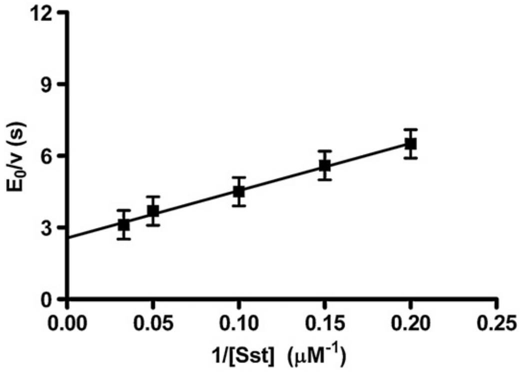

Fig. 3. Kinetics of hydrolysis of somatostatin by IDE. Lineweaver–Burk double-reciprocal plot of the degradation of somatostatin by IDE at 37 °C and pH7.3. Catalytic parameters were obtained employing Eq. (3) and are reported in Table 1. Indicated concentrations of somatostatin were incubated with 10 nM IDE in 0.1 M phosphate buffer at pH7.3 and 37 °C. Aliquots were taken at different time intervals (i.e., 0 h, 15 min, 30 min, 1 h, 3 h, 5 h) and the reactions were stopped with EDTA (0.5 mM). Samples were analyzed with reverse-phase HPLC.

Kinetic parameters analysis reveals that the enzymatic processing of somatostatin by IDE is less efficient than that for FβA (as from values of k_{cat}/K_m in Table 1) because of the very slow rate-limiting step k_{cat} (see Table 1), even though the IDE–somatostatin affinity is much higher (as from K_m in Table 1). It has been observed that somatostatin spontaneously self-assembles into a wide molecular range of aggregates and even fibrils.[28] However, since IDE has been reported to hydrolyze only peptides with molecular mass <6 kDa,[9] it means that IDE should able to hydrolyze only low-molecular-mass species of somatostatin, corresponding to either monomers or small oligomeric forms (up to 6 kDa). Therefore, the high affinity observed for the interaction with IDE (as from the very low K_m value, see Table 1) indicates that oligomerization does not seem to impair the recognition by IDE, while the quite slow k_{cat} (see Table 1) might underlie the possibility that the cleavage process is somehow affected by the assembly into small oligomers.

Mass spectrometry identification of somatostatin cleavage site

In order to identify cleavage site(s) on somatostatin sequence, we performed mass spectrometry (MS) studies. In Fig. 4, the mass spectrum of 15 μM somatostatin in phosphate-buffered saline (PBS) buffer in the presence or absence of 18 nM IDE is reported. Somatostatin is identified as the molecular peak at m/z 1637.5 (Fig. 4a); other signals, attributed to somatostatin, appear in the spectrum mainly due to the high salt content (Na^+, K^+) of the solution (m/z 1659.7, m/z 1676.0). Somatostatin dimeric species containing one, two, or three K^+ ions also appear at m/z 3317.5, 3361.9, and 3393.3, respectively. After 1 h incubation of somatostatin with IDE at 37 °C, new peaks appear in the spectrum (Fig. 4b), namely, at m/z 639.5, 1019.1, 1321.4, 1654.8, 2677.9, and 3356.6. The two most intense peaks at m/z 1654.8 and 3356.6 are easily assigned to cleaved monomeric and dimeric somatostatin molecules, respectively. Thus, since somatostatin is a cyclic peptide, these peaks can be attributed to the monomeric and dimeric forms, respectively, of the cleaved somatostatin molecules, which are in the "open ring" conformation with an additional water molecule at the site cleaved by IDE. In order to confirm this assignment, to identify the remaining peaks and to establish the exact location of the cleavage site, it was necessary to carry out MS/MS experiments accompanied by a reduction/alkylation step before the MS analysis.[29] The presence of two peaks at m/z 696.2 and 1076.3 in the mass spectrum of the reduced/alkylated solution followed by MS/MS identification (data not shown) allowed us to assign the two peaks at m/z 639.5 and 1019.1 as fragments of degraded somatostatin in which the disulfide bond between Cys3 and Cys14 was reduced and broken, as reported in Table 2. The unambiguous identification of these fragments allowed us to identify the cleavage site at the Phe6–Phe7 amino acid bond.

Interaction of IDE with somatostatin

Surface plasmon resonance measurements

The interaction between IDE and somatostatin was investigated by surface plasmon resonance imaging

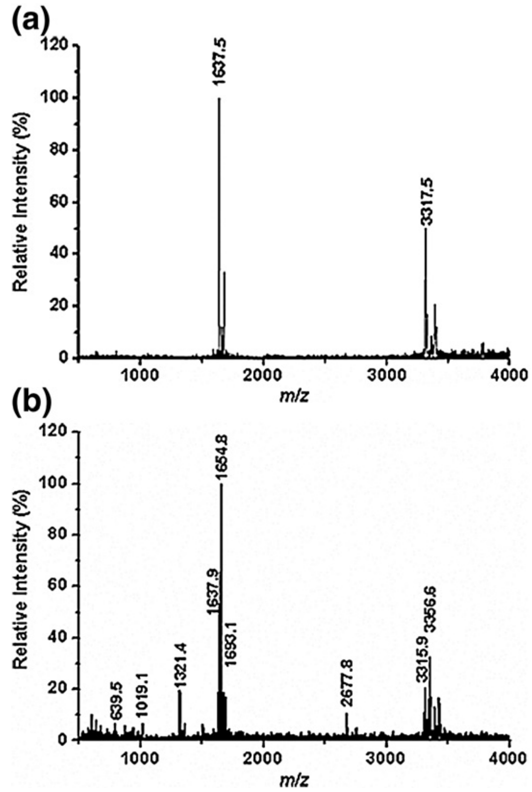

Fig. 4. AP-MALDI mass spectra of somatostatin samples. Somatostatin (15 μM) in PBS buffer was incubated in the absence (a) or presence (b) of 18 nM IDE at 37 °C for 1 h.

Table 2. Somatostatin fragments produced by IDE

	Calculated peaks (m/z)	Experimental peaks (m/z)	Calculated alkylated peaks (m/z)	Experimental alkylated peaks (m/z)
HalaGlyCysLysAsnPheOH	639.7	639.5	696.7	696.2
HPheTrpLysThrPheThrSerCysOH	1019.7	1019.1	1076.7	1076.3

(SPRI) technique, and in Fig. 5, the SPRI kinetic data are reported for three somatostatin solutions flowing into different microchannels at various concentrations (flow rate = 50 μl/min). In order to give an insight into the mechanism of such an interaction, a common way to proceed is to find the theoretical interaction model that best fits the experimental kinetic curves.[30,31] In our case, best results were obtained with an interaction model considering two different sites to be present onto the interacting surface. Rate and equilibrium constants derived from the fitting of the experimental kinetic data are shown in Table 3. These data result from a biphasic interaction of the somatostatin with the surface-immobilized IDE. In fact, the two different affinity constant values [$K_1 = 4.9\ (\pm 2.2) \times 10^5\ \mathrm{M}^{-1}$, $K_2 = 1.6\ (\pm 0.8) \times 10^5\ \mathrm{M}^{-1}$] indicate (i) the presence of two different sites on the IDE surface, which are characterized by fairly similar affinities for somatostatin, and/or (ii) the possibility that various assembly forms of somatostatin display slightly different kinetic parameters with IDE. Unfortunately, at this stage, we cannot discriminate between these two hypotheses; neither can we rule out the possibility that the two equilibrium constants observed by SPR experiments (K_1 and K_2, see Table 3) might have originated from some heterogeneity in the enzyme surface after the IDE immobilization on the SPR chip.

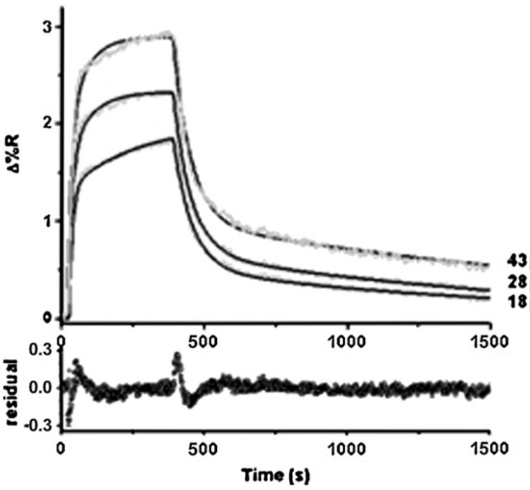

Fig. 5. SPRI results. SPRI kinetic data for the interaction between immobilized IDE and somatostatin at the concentrations indicated (gray lines). Curves resulting from the fitting obtained adopting the surface heterogeneity model are shown in black. Residuals are also shown (bottom part, dotted lines). Experimental conditions are described in the text.

Under such an assumption, the similar values calculated for K_1 and K_2 result from surface effects affecting the functioning of the immobilized IDE and represent the affinity of somatostatin to surface-immobilized IDE molecules having slightly different local arrangements. However, it must be outlined that one of the two equilibrium constants (namely, K_2, see Table 3) is similar to the reciprocal of the Michaelis–Menten constant from enzymatic cleavage of somatostatin [i.e., $1/K_m = 1.3\ (\pm 0.2) \times 10^5\ \mathrm{M}^{-1}$, see Table 1], suggesting that (i) both parameters refer to the interaction of somatostatin with free IDE and (ii) K_m closely corresponds to the equilibrium dissociation constant for the somatostatin substrate with free IDE.

In order to decouple the binding process from the enzymatic activity, we have also carried out binding experiments of somatostatin to IDE inactivated by exposure to ethylenediaminetetraacetic acid (EDTA), which chelates the catalytic Zn^{2+} ion, abolishing the enzymatic activity of IDE. It is interesting to observe that inactivation of IDE brings about a drastic (about 10-fold) reduction of somatostatin affinity, which is exerted through a dramatic increase of the dissociation rate constant, whereas the association rate constant remains essentially unperturbed (see Fig. S3).

Circular dichroism measurements

In order to monitor the structural changes induced by the somatostatin–IDE interaction, we performed circular dichroism (CD) spectroscopy of the enzyme in the absence or in the presence of indicated concentrations of somatostatin (Fig. 6a). The same experiments were performed in the presence of EDTA, which is known to inactivate IDE by removing the

Table 3. Equilibrium constants for somatostatin binding to IDE as from CD, activity effect, and surface plasmon resonance

Circular Dichroism	
K_a (M^{-1})	$1.2\ (\pm 0.2) \times 10^5$
K_b (M^{-1})	$4.9\ (\pm 0.5) \times 10^3$
Activity effect	
K (M^{-1})	$1.3\ (\pm 0.2) \times 10^5$
Surface plasmon resonance	
k_{1a} ($\mathrm{M}^{-1}\ \mathrm{s}^{-1}$)	$3.4\ (\pm 1.4) \times 10^2$
k_{1d} (s^{-1})	$7.0\ (\pm 1.5) \times 10^{-4}$
K_1 (M^{-1})	$4.9\ (\pm 2.2) \times 10^5$
k_{2a} ($\mathrm{M}^{-1}\ \mathrm{s}^{-1}$)	$2.4\ (\pm 1.3) \times 10^3$
k_{2d} (s^{-1})	$1.5\ (\pm 0.2) \times 10^{-2}$
K_2 (M^{-1})	$1.6\ (\pm 0.8) \times 10^5$

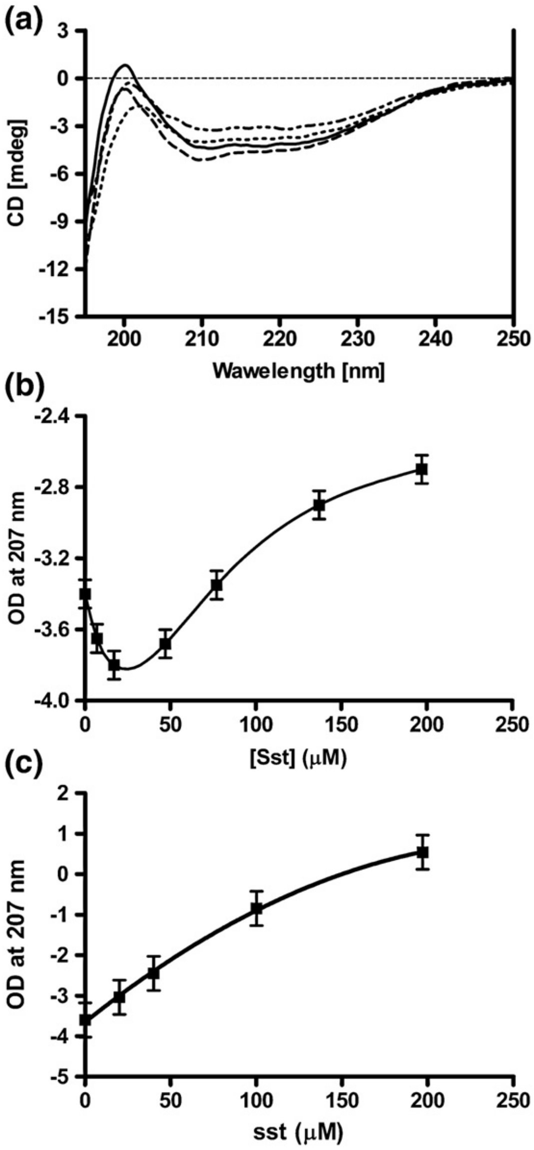

Fig. 6. Conformational changes in IDE structure mediated by somatostatin. (a) CD spectroscopy of 1 μM IDE in 40 mM phosphate buffer at 37 °C in the absence and in the presence of different somatostatin concentrations: 0 μM (——), 40 μM (– – –), 80 μM (- - -), and 200 μM (–..–..–). (b) The somatostatin concentration-dependent effect on the ellipticity signal of IDE at 207 nm. Continuous line was obtained from the nonlinear least-squares fitting of data according to Eq. (1), employing the values of K_a and K_b reported in Table 3. (c) The somatostatin effect on IDE inactivated with EDTA at 207 nm. The continuous line corresponds to a single binding curve characterized by a $K_{EDTA} = K_b$ in Table 3.

catalytic Zn^{2+} ion. It is important to highlight that, due to somatostatin enzymatic processing by IDE, a fraction of somatostatin is cleaved during the time required for the spectra collection. This amount (calculated on the basis of the time interval and the catalytic parameters reported in Table 1) has been subtracted from the somatostatin concentration employed for the quantitative analysis (see below), under the assumption that cleaved somatostatin does not interact with IDE. Binding of somatostatin can be followed as a concentration-dependent variation of CD spectra of IDE in the near-UV region, suggesting a structural variation of the helical arrangement of the enzyme. From Fig. 6a, it comes out that addition of somatostatin at first induces (up to 50 μM somatostatin) an increase of the negative ellipticity in the 207- to 222-nm region, followed at higher concentrations by a decrease of the negative ellipticity. This behavior may be described by a two-site binding process; therefore, a quantitative analysis of concentration-dependent binding of somatostatin to IDE was performed based on the ellipticity values at 207 nm (Fig. 6b) according to the following mechanism:

$$E + L \overset{K_a}{\rightleftharpoons} \mathrm{EL}_1 + L \overset{K_b}{\rightleftharpoons} \mathrm{EL}_2 \qquad \text{(Scheme1)}$$

where K_a and K_b are affinity constants for somatostatin binding to E and EL_1, respectively (Table 3).

According to Scheme 1, K_a and K_b were calculated by fitting of experimental data to the following equation,

$$S_{obs} = S_E \frac{1}{1 + K_a \cdot [\mathrm{Sst}] + K_a \cdot K_b \cdot [\mathrm{Sst}]^2} + S_{EL1} \frac{K_a \cdot [\mathrm{Sst}]}{1 + K_a \cdot [\mathrm{Sst}] + K_a \cdot K_b \cdot [\mathrm{Sst}]^2} + S_{EL2} \frac{K_a \cdot K_b [\mathrm{Sst}]^2}{1 + K_a \cdot [\mathrm{Sst}] + K_a \cdot K_b \cdot [\mathrm{Sst}]^2} \qquad (1)$$

where S_{obs} is the observed ellipticity signal; S_E, S_{EL1}, and S_{EL2} are the ellipticity signals of the three species reported in Scheme 1; K_a and K_b are the affinity constants of somatostatin to the species E and EL_1, respectively; and [Sst] is the somatostatin concentration. The values of K_a and K_b, reported in Table 3, suggest that binding of somatostatin to the high-affinity site is accompanied by an increase of secondary and tertiary structural compactness. Furthermore, at increasing somatostatin concentrations, it interacts with an additional lower-affinity binding site of IDE, inducing a partial loss of the structural arrangement of the whole enzyme, as represented by the marked reduction of the negative ellipticity signal (Fig. 6a). It is interesting to observe that the high-affinity equilibrium constant [i.e., $K_a = 1.2\ (\pm 0.2) \times 10^5\ \mathrm{M}^{-1}$, see Table 3] is closely similar to $1/K_m$, obtained from the somatostatin enzymatic processing by IDE (see Table 1), and to K_2 obtained from SPR experiments (see Table 3), clearly indicating that these equilibrium constants all refer to the same molecular process, which corresponds to the interaction of free IDE with somatostatin.

On the other hand, the lower-affinity constant K_b observed by CD has no counterpart in the enzymatic activity of IDE on somatostatin (see Fig. 3) or in the interaction followed by SPR (see Fig. 5). It likely refers instead to the interaction of somatostatin with a lower-affinity binding pocket distinct from the substrate active site, which brings about an alteration of the tertiary (and likely quaternary) structure of IDE. This assumption is also supported by the evidence that IDE inactivated by EDTA displays the same low-affinity equilibrium constant for somatostatin as the active IDE (i.e., $K = K_b = 4.9 \times 10^3\ M^{-1}$, see Table 3), inducing only a loss of the structural arrangement of the enzyme (Fig. 6c). As a whole, data by SPR and CD both seem to confirm that upon inactivation by EDTA, the high-affinity site for somatostatin (possibly the active site) dramatically reduces its binding affinity, either becoming unable to bind somatostatin or displaying a value similar to the low-affinity site.

Effect of somatostatin on IDE processing of the amyloid peptide

The effect of human somatostatin on the IDE-dependent degradation of fluorogenic substrate was measured in reaction mixtures containing 5 μM FβA peptide and 2 nM IDE in the presence of indicated concentrations of somatostatin. It is important to underline that, due to the somatostatin enzymatic processing by IDE, a fraction of somatostatin is cleaved during the time required for the fluorogenic assay. This amount (calculated on the basis of the time interval and the catalytic parameters reported in Table 1) has been subtracted from the somatostatin concentration employed for the quantitative analysis (see below), under the assumption that cleaved somatostatin does not interact with IDE. The enzymatic activity on FβA as a function of somatostatin concentration is compared with values obtained in the absence of somatostatin (Fig. 7). Somatostatin significantly enhances IDE activity, with the maximum effect at about 40 μM, a behavior perfectly consistent with the spectroscopic effect observed by CD (Fig. 6), suggesting that this effect is related to the binding of somatostatin to free IDE. It is interesting to outline that the same effect has also been observed in the case of other IDE substrates, such as β-endorphin, bradykinin, and several dynorphins.[10] Like for some of these substrates, at a much higher somatostatin concentration (>100 μM), an inhibitory effect is observed (Fig. 7), likely due to the presence in the FβA cleavage site of a second somatostatin molecule, which becomes, in this way, a competitive inhibitor. It is worth outlining that this concentration range is closely similar to that observed for the lower-affinity constant observed by CD, suggesting that this interaction is also responsible for the progressive disappearance of the somatostatin-linked activation process. However, since the inhibitory effect appears at very high somatostatin concentrations, we have only analyzed the enhancing effect according to the following equation:

$$A_{obs} = \frac{1}{1 + K \cdot [\mathrm{Sst}]} + A_r \frac{K \cdot [\mathrm{Sst}]}{1 + K \cdot [\mathrm{Sst}]} \qquad (2)$$

where A_{obs} is the observed relative activity with respect to IDE in the absence of somatostatin, A_r is the relative activity in the presence of a somatostatin concentration needed to saturate the binding site, K is the somatostatin affinity binding constant, and [Sst] is the somatostatin concentration. This equation underlies the existence of only one activating binding site for somatostatin, as it appears from our data over the investigated concentration range.

The close similarity of the somatostatin high-affinity constant from CD experiments (i.e., K_a in Table 3, see Fig. 6) with both the equilibrium constant for the second binding site observed by SPRI experiments (i.e., K_2 in Table 3, see Fig. 7) and that resulting from the rate-enhancing effect (i.e., K in Table 3, see Fig. 7) indeed suggests that (i) the high-affinity site by CD (corresponding to the binding site characterized by K_2 in SPRI experiments) is a modulatory cleft and (ii) the activity effect is related to the interaction of somatostatin with free IDE (i.e., E in Scheme 1). In addition, the catalytic parameters, obtained for FβA processing by IDE in the presence of 40 μM somatostatin (see Fig. 2), show that the somatostatin-linked effect is only exerted on K_m, leaving k_{cat} unchanged (see Table 1). Therefore, the rate-enhancing effect (see Fig. 7) is due to an allosteric mechanism, such that the binding of somatostatin to one site brings about a conformational change of a second site, facilitating the FβA binding. However, this conformational change affects the substrate affinity (as from the decrease of K_m for FβA upon somatostatin addition) but it does not change the cleavage rate k_{cat}. This has already been observed for the processing of a synthetic substrate in the presence of dynorphin B-9,[10] suggesting that cooperativity in IDE is likely expressed mostly through a change of substrate affinity without affecting significantly the speed of the rate-limiting step.

Discussion

IDE is a Zn^{2+} metalloprotease characterized by the presence of different quaternary structures (namely, monomeric, dimeric, and tetrameric forms), which might display different enzymatic activity toward amyloidogenic proteins.[1,10] It has been shown that IDE is able to enzymatically process the amyloid β-protein,[32] giving rise to new fragments that are not neurotoxic or that do not deposit on amyloid plaques[25,33] and that this activity can be modulated by metabolic peptides, such as dynorphins.[1] As a whole, these findings render IDE a potentially interesting target for the design of anti-Alzheimer's drugs.[34,35]

Furthermore, it is well known that somatostatin performs crucial roles in the brain and that its decrease represents a pathological feature of AD, even though this reduction is not accompanied by an alteration of proteolytic processing of peptide precursors.[36] Although the mechanism that couples alterations of the somatostatinergic system to AD remains unclear, recently, it has been shown that somatostatin regulates β-amyloid metabolism

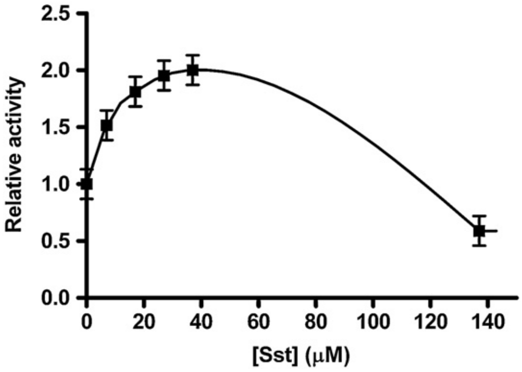

Fig. 7. Effect of somatostatin on IDE-catalyzed hydrolysis of FβA. Hydrolysis of 5 μM FβA by 10 nM IDE was followed as a function of the concentration of somatostatin in 40 mM phosphate buffer at pH7.3 and 37 °C. Activity is plotted in relation to the values obtained in the absence of somatostatin. The continuous line between 0 somatostatin and 40 μM somatostatin was obtained by nonlinear least-squares fitting of data according to Eq. (2), and the value of K is reported in Table 3. The continuous line connecting the experimental point at 40 μM somatostatin with the point at 140 μM somatostatin is simply drawn, and it does not correspond to a nonlinear least-squares fitting.

through the modulation of neprilysin proteolytic activity.[19,23,24]

In this work, we show for the first time that the neuropeptide somatostatin is not only a novel substrate of IDE but also a modulator of its activity toward a FβA peptide, corresponding to the 10–25 amino acid sequence of the Aβ(1–40), which displays a behavior quite similar to that observed for the intact Aβ(1–40) (see Fig. 7 and Tables 1 and 3). IDE is able to hydrolyze it at the Phe6–Phe7 bond (see Table 2), confirming that IDE cleaves preferentially peptides showing self-assembly properties, involving basic and/or hydrophobic amino acids.[11,28] Although the factors responsible for its "*in vivo*" degradation in the brain remain largely unknown, it has been shown that somatostatin is degraded by membrane-associated forms of other Zn-proteases, such as neurolysin and thimet endopeptidase,[26,27] displaying multiple cleavage sites. Here, we show that, indeed, one of these sites is in common with that of IDE (see Fig. S4), suggesting the possibility that in a physiological environment, the single IDE cleavage on somatostatin may not generate two fragments but an open ring of somatostatin, which could facilitate its enzymatic processing by other enzymes. Therefore, the somatostatin degradation pattern probably involves several enzymes in the brain, making extremely interesting a further investigation on the molecular and physiological interrelationships between them.

The close similarity between the higher-affinity equilibrium constant of somatostatin for IDE observed by CD (i.e., K_a in Table 3) and the reciprocal of the K_m from its enzymatic processing by IDE (see Tables 1 and 3) reveals that the interaction of somatostatin with one of the active sites of the oligomeric IDE (which has been proposed to be predominantly in the dimeric form under normal steady-state enzymatic conditions)[10] induces changes in the secondary and tertiary conformation(s), as from CD spectra (Fig. 6a). The kinetics of this interaction (see Fig. 5 and Table 3) indicates that the process is relatively slow and the complex is stable (as from the fairly slow dissociation rate constant k_{2d} in Table 3). However, it must be underlined that the removal of the catalytic Zn^{2+} ion after exposure of IDE to EDTA brings about a conformational change, which decreases dramatically the ligand affinity. This is supported by both the enhanced somatostatin dissociation rate constant, observed by SPR (see Fig. S3), and the disappearance of the higher-affinity site for somatostatin (characterized by the equilibrium constant $K_a = 1.2 \times 10^5\ M^{-1}$, see Fig. 6b and Table 3). The low-affinity site does not seem instead affected by the EDTA-induced inactivation of IDE (see Fig. 6c). It is very important to outline that the binding of a small ligand substrate molecule (such as somatostatin) to IDE is accompanied by relevant changes of its secondary and tertiary structure (as from CD experiments). This clearly indicates that the enzyme undergoes an induced-fit ligand-linked conformational transition, which is associated to an increased enzymatic activity, as indicated by the enhanced rate of FβA peptide processing (see Fig. 7). This allosteric effect is exerted through a decrease of K_m for the FβA peptide processing by IDE (see Fig. 2), leaving essentially unchanged the speed of the rate-limiting step k_{cat} (see Table 1). Therefore, in the framework of an allosteric mechanism,[37] we can exploit the ligand-linked variation of K_m to calculate the interaction energy (ΔG_I) between the active sites ($\Delta G_I = RT\Delta \ln K_m$), which turns out to be ligand dependent, since it is smaller and similar for somatostatin (see Table 1) and β-endorphin and somewhat larger for bradykinin and dynorphins.[10]

The binding of a second somatostatin molecule to IDE (which displays a much lower affinity, as from K_b in Table 3 and Fig. 6) must necessarily occur at a topologically different site, which is unlikely to be a catalytic one (as also suggested by the lack of an effect after the EDTA-induced inactivation of IDE), since no evidence for a slower enzymatic process of somatostatin by IDE is observed at larger substrate concentrations (data not shown). This binding brings about a widespread structural change of IDE (as detected by CD, see Fig. 6), possibly involving also the quaternary arrangement of IDE, which results in a decreased enzymatic activity at higher somatostatin concentrations (see Fig. 7).

These observations contribute to elucidate IDE–somatostatin interaction and the modulating role of somatostatin in the brain. This interaction may have important physiopathological consequences, since under physiological conditions, somatostatin could facilitate β-amyloid degradation in somatostatin-positive neurons, preventing the deposition of amyloid plaques; in addition, IDE could contribute to control somatostatin levels through its enzymatic action on it.

As a whole, this complex regulatory mechanism may represent an elegant feedback network, which may play a central role in the homeostasis of somatostatin and β-amyloid. Thus, although a biological counterproof is needed, we can hypothesize that the brain levels of somatostatin and β-amyloid may be mutually balanced by the IDE enzymatic activity on both of them and by their reciprocal modulatory role on the IDE enzymatic activity. A pathological decrease of somatostatin synthesis may break this balance and could trigger a down-regulation of IDE and neprilysin activity with a consequent accumulation of β-amyloid, leading to a vicious cycle that could be crucial for the onset of neurodegenerative processes.[38]

Materials and Methods

Materials

Recombinant IDE was obtained from Calbiochem. Human somatostatin, ethanol solution, ethanolamine–HCl (1 M), guanidine–HCl (8 M), and dithiobis(*N*) succinimidylpropionate (Lomant's reagent) were all purchased from Sigma-Aldrich (Milan, Italy). Dithiol tethers SPT-0013 and SPT-0014C were purchased from Sensopath. Gold substrates (GWC Technologies, USA) were obtained by thermally evaporating a gold layer (450 Å) onto SF-10 glass slides (Schott, USA). Chromium (50 Å) was used as the adhesion layer. IDE preparations were in 40 mM phosphate buffer at pH7.3 and somatostatin preparations were in 0.1 M phosphate buffer at pH7.3. Classical fluorenylmethoxycarbonyl (Fmoc)-protected amino acid derivatives, the KA amide TentaGel resin, the protected Fmoc-L-Glu{5-[(2-aminoethyl)-amino]naphthalene-1-sulfonic acid (EDANS)}-OH, and the [4-((4-(dimethyl-amino) phenyl)azo)benzoic acid]-*N*-hydroxysuccinimide ester (Dabcyl-OSu) for the synthesis of the peptide were from Novabiochem (Laufelfingen, CH). Solvents were from ROMIL (Dublin, Ireland); other reagents for peptide synthesis, such as piperidine, activating agents, diisopropyl ethylamine, trifluoroacetic acid (TFA), and triisopropylsilane were from Sigma-Aldrich.

FβA peptide synthesis

The internally quenched novel peptide,[39] derived from Aβ(1–40), Dabcyl-Tyr-Glu-Val-His-His-Gln-Lys-Leu-Val-Phe-Phe-Ala-Glu-Asp-Val-Gly-Glu(EDANS)-NH2 (FβA), and containing residues 10–25, was prepared on a 433A Applied Biosystems automatic synthesizer (synthesis scale: 0.1 mmol), following standard Fmoc/tBu protocols of solid-phase peptide synthesis.[40] Briefly, the peptide was assembled on a RINK amide PEGA resin onto which Fmoc-L-Glu(EDANS)-OH was previously anchored. All amino acid derivatives were preactivated with 1-H-benzotriazolium, 1-[bis(dimethylamino)methylene]-hexafluorophosphate(1-),3-oxide/*N*-hydroxybenzotriazole and coupled for 30 min. Deprotection of the Fmoc group was achieved by treatment with 30% piperidine in dimethyl formamide for 20 min. Following the insertion of the N-terminal residue and deprotection, the Dabcyl group was introduced by treatment of the resin with Dabcyl-OSu (10 eq.) in dimethyl formamide (0.5 M) in the presence of diisopropyl ethylamine (20 eq.). The peptide was cleaved from the resin by treatment with a TFA–H_2O–triisopropylsilane (90:5:5, v/v/v) mixture for 4 h at room temperature, precipitated in cold diethylether, and lyophilized from a 50:50 H_2O–CH_3CN solution. The crude product was purified to homogeneity by semipreparative RP-HPLC using a C18 50×2.2 cm ID column (Phenomenex, Torrance, CA) equilibrated at 20 ml/min with 20% CH_3CN in H_2O and 0.1% TFA. A gradient from 20% to 70% CH_3CN and 0.1% TFA was applied for 50 min to elute the peptide. Fractions containing the purified product were pooled, and the product was then characterized by liquid chromatography (LC)–MS on an LCQ Deca XP Ion Trap mass spectrometer (ThermoElectron, Milan, Italy) equipped with an OPTON ESI source, operating at 4.2 kV needle voltage and 320 °C and with a complete Surveyor HPLC system. Narrow-bore 50×2 mm C18 BioBasic LC–MS columns from ThermoElectron equilibrated at 0.2 ml/min with 20% CH_3CN in H_2O and 0.05% TFA were used for these analyses. A gradient from 20% to 70% of CH_3CN and 0.05% TFA over 50 min was applied to elute the peptide. The molecular weight was consistent with the expected value within the limits of the experimental error ($MW_{Exp/Theor}$: 2545.6/2545.72 amu).

The FβA was dissolved in 20 mM phosphate buffer and 50% dimethyl sulfoxide, pH7.3. Undissolved species were removed by centrifuging freshly dissolved peptide at 10,000*g* for 2 h at 4 °C, and the resulting supernatant was stored at −20 °C until use.[41] Peptide concentrations were determined using EDANS's extinction coefficient of 5.9 mM^{-1} cm^{-1} at 335 nm.

Methods

HPLC analysis

Reaction mixtures containing 10 nM IDE and increasing concentrations of somatostatin were incubated at 37 °C for 5 h in 0.1 M phosphate buffer, pH7.3. Aliquots were taken at different time intervals (i.e., 0 h, 15 min, 30 min, 1 h, 3 h, 5 h), and the reaction was stopped by addition of 0.5 mM EDTA. Samples were applied to a C4 reverse-phase HPLC column (Surveyor, Thermo Finnigan), and the elution was performed at a flow rate of 1 ml/min using a linear gradient: 95% eluent A (H_2O+0.1% TFA) and 5% eluent B (CH_3CN+0.1% TFA), with absorbance monitored at 220 and 254 nm.

Mass spectrometry: AP-MALDI MS experiments

Reaction mixtures containing 18 μM somatostatin in the presence or absence of 10 nM IDE in 0.1 M phosphate buffer (pH7.3) were incubated at 37 °C for 1 h and analyzed with atmospheric pressure matrix-assisted laser desorption/ionization (AP-MALDI) MS.

All the AP-MALDI MS experiments were carried out by using a Finnigan LCQ Deca XP PLUS (Thermo Electron Corporation, USA) ion trap spectrometer that was fitted with a MassTech Inc. (USA) AP-MALDI pulsed dynamic focusing source. The latter consists of a flange containing a computer-controlled X–Y positioning stage and a digital camera and is powered by a control unit that includes a pulsed nitrogen laser (wavelength, 337 nm; pulse width, 4 ns; pulse energy, 300 μJ; repetition rate up to 10 Hz) and a pulsed dynamic focusing module that imposes a delay of 25 μs between the laser pulse and the application of the high voltage to the AP-MALDI target plate. Laser power was attenuated to about 55%. The target plate voltage was 1.8 kV. The ion trap inlet capillary temperature was 220 °C. Capillary and tube lens offset voltages of 30 and 15 V, respectively, were applied. Other mass spectrometer parameters were as follows: multipole 1 offset at −3.75 V, multipole 2 offset at −9.50 V, multipole radio-frequency (RF) amplitude 400 V, lens at −24.0 V, and entrance lens at −88.0 V. Automatic Gain Control was turned off and instead the scan time was fixed by setting the injection time to 220 ms and using five microscans. Although there is the risk of losing resolution, the latter experimental conditions were chosen as sensitivity was the main goal in most experiments. For the same reason, although 1 min acquisition per sample was usually performed, in some cases, it was necessary that an acquisition up to 5 min and different experiments were reproduced from three to five times.

Spectra of the studied solutions were acquired in a data-dependent fashion by first acquiring full extended mass range from m/z 200 to 4000, followed by MS/MS scans of the most intense ions of the previous full MS scan. MS/MS scans were acquired using an isolation width of 5 m/z, activation q_z of 0.250, activation time of 30 ms, and normalized collision energy (NCE) in the range 30–40%, dependent on the ion {NCE is the amplitude of the resonance excitation RF voltage scaled to the precursor mass based on the following formula: RF amplitude = [NCE%/30%] (precursor ion mass × tick amp slope + tick amp intercept), where the tick amp slope and tick amp intercept are instrument-specific values. For our LCQ Deca, 35% NCE for m/z 1000 = 1.8 V}.

In order to unambiguously assign the somatostatin fragments produced by IDE, a reduction/alkylation step was carried out in the reaction mixture prior to the MS analysis without any purification step, according to the procedure previously described.[29]

Fluorogenic assay for FβA hydrolysis by IDE

The hydrolysis of the fluorogenic peptide was measured at 37 °C following the increase in fluorescence at 472 nm (with excitation at 336 nm) after cleavage of the peptide bond by IDE and the separation of the quenching Dabcyl group from the fluorescent EDANS group. Reaction mixtures contained the fluorogenic peptide substrate at the indicated concentrations and 10 nM IDE.

The effect of somatostatin on the IDE activity was investigated following the hydrolysis of FβA at 37 °C in a reaction mixture containing either (i) 2 nM IDE, 5 μM FβA, and various concentrations of human somatostatin or (ii) 40 μM somatostatin, 2 nM IDE, and indicated FβA concentrations. The reactions were followed on a Cary Eclipse fluorescence spectrofluorometer.

CD spectroscopy

IDE was diluted to 1 μM in 40 mM phosphate buffer at pH7.3 in the absence and in the presence of different concentrations of somatostatin. The same experiments were performed in the presence of 50 μM EDTA. Samples were examined using 0.2-mm quartz cuvettes in a Jasco J-720 CD spectropolarimeter (Tokyo, Japan). Spectra were recorded at 37 °C and at 1 nm resolution with a scan rate of 20 nm/min. Eight scans were acquired and averaged for each sample.

Poly(dimethylsiloxane) microfluidic devices fabrication

Microfluidic devices were made in poly(dimethylsiloxane) (PDMS) polymer as described elsewhere.[42] Briefly, PDMS microchannels were created by replication from masters in polyvinyl chloride. Replicas were formed from a 1:10 mixture of PDMS curing agent and prepolymer (Sylgard 184, Dow Corning, USA). The mixture was degassed under vacuum and then poured onto the master in order to create a layer with a thickness of about 3–4 mm. The PDMS was then incubated for at least 2 h at 60 °C before being removed from the masters. Microchannels were 500 μm wide and 80 μm in height. At the ends of each channel, there were circular reservoirs (diameter, 400 μm). PEEK tubes (Upchurch Scientific) were inserted in such reservoirs in order to connect the PDMS microfluidic cell to an Ismatec IP-N (Ismatec SA, Switzerland) peristaltic pump.

SPRI measurements

The SPRI apparatus (GWC Technologies, USA) and the microfluidic system used were the same as reported in some of our previous works.[43] A six-microchannel microfluidic device was used in this case to follow the interaction between IDE and somatostatin at different concentrations.

SPR images were analyzed by using the V++ software (version 4.0, Digital Optics Limited, New Zealand) and the software package Image J 1.32j (National Institutes of Health, USA). SPRI provides data as pixel intensity units (0–255 scale). Data were converted in percentage of reflectivity (%R) by using the formula:

$$\%R = 100^{*}\left(0.85\, I_{\mathrm{p}}/I_{\mathrm{s}}\right)$$

where I_p and I_s refer to the reflected light intensity detected using p- and s-polarized light, respectively.

Experiments were carried out by sequentially acquiring 15 frame-averaged SPR images with 5 s time delay between them. Kinetic data were obtained by plotting the difference in percent reflectivity (%R) from selected regions of interest of the SPR images as a function of time. All the SPRI experiments were carried out at room temperature. The rate constants k_a and k_d were calculated by fitting adsorption/desorption kinetics data through numerical integration analysis.[44]

Immobilization of IDE on gold surface

Two different immobilization procedures were scrutinized for IDE and positive results were obtained in both cases. Specifically, similar SPRI signals were indeed registered after a 40-min injection at 5 μl/min of a 36-nM IDE solution into a microchannel in contact with a gold surface previously functionalized with (a) Lomant's reagent[45] and (b) dithiol tethers (SPT-0013:SPT-0014C = 10:1 mixed ethanol solution).[46] The same procedure was followed with IDE previously inactivated by EDTA.

We found that the pH of the PBS buffer used for sample dilution is crucial for a positive result of the activity measurements and a pH of 7.3 was chosen for all experiments. Ethanolamine–HCl (1 M) was used for deactivation of the unreacted NHS groups, while 5 min injection at 5 μl/min of guanidine–HCl (8 M) was used for the denaturation of IDE. This last procedure was undertaken to avoid the possibility that observed signals were due to unspecific interactions between the somatostatin molecules and the functionalized SPRI chips. Thus, a large difference in the SPRI signal was recorded according to whether the somatostatin solutions were injected into microchannels where the immobilized IDE was in the native form or it had been previously denatured (see Fig. S5). This result reinforces the conclusion that the kinetic data recorded in the case of active IDE–somatostatin are due to a real interaction between somatostatin and IDE rather than to trivial somatostatin unspecific interactions with the functionalized SPRI chip.

Acknowledgements

The authors thankfully acknowledge useful discussions with Prof. S. Marini and Drs. G. F. Fasciglione and D. Di Pierro during the early stages of the project. The financial contribution from the Italian Ministry of University and Research (MiUR FIRB RBNE03PX83 to M.R., E.R., and M.C.) is gratefully acknowledged.

Supplementary Data

Supplementary data associated with this article can be found, in the online version, at doi:10.1016/j.jmb.2008.11.025

References

1. Song, E.-S. & Hersh, L. B. (2004). Insulysin. *J. Mol. Chem.* **5**, 201–220.
2. Duckeorth, W. C., Bennett, R. G. & Hamel, F. G. (1998). Insulin degradation: progress and potential. *Endocr. Rev.* **19**, 608–624.
3. Leissring, M. A., Farris, W., Wu, X., Cristodoulou, D. C., Haigis, M. C., Guarente, L. & Selkoe, D. J. (2004). Alternative translation initiation generates a novel isoform of insulin-degrading enzyme targeted to mitochondria. *Biochem. J.* **383**, 439–446.
4. Qiu, W. Q. & Folstein, M. F. (2006). Insulin, insulin-degrading enzyme and amyloid-β peptide in Alzheimer's disease: review and hypothesis. *Neurobiol. Aging*, **27**, 190–198.
5. Bertram, L., Blacker, D., Mullin, K., Keeney, D., Jones, J., Basu, S. *et al.* (2000). Evidence for genetic linkage of Alzheimer's disease to chromosome 10q. *Science*, **290**, 2302–2303.
6. Ghosh, S., Watanabe, R. M., Valle, T. T., Hauser, E. R., Magnuson, V. L., Langefeld, C. D. *et al.* (2000). The Finland–United States investigation of non-insulin-dependent diabetes mellitus genetics (FUSION) study. I. An autosomal genome scan for genes that predispose to type 2 diabetes. *Am. J. Hum. Genet.* **67**, 1174–1185.
7. Meigs, J. B., Panhuysen, C. I., Myers, R. H., Wilson, P. W. & Cupples, L. A. (2002). A genome-wide scan for loci linked to plasma levels of glucose and HbA(1c) in a community-based sample of Caucasian pedigrees: the Framingham offspring study. *Diabetes*, **53**, 833–840.
8. Shen, Y., Joachimiak, A., Rosner, M. R. & Tang, W. J. (2006). Structure of human insulin-degrading enzyme reveals a new substrate recognition mechanism. *Nature*, **443**, 870–874.
9. Im, H., Manolopoulou, M., Malito, E., Shen, Y., Zhao, J., Fery, M. N. *et al.* (2007). Structure of substrate-free human insulin-degrading enzyme and biophysical analysis of ATP-induced conformational switch of IDE. *J. Biol. Chem.* **282**, 25453–25463.
10. Song, E.-S., Juliano, M. A., Juliano, L. & Hersh, L. B. (2003). Substrate activation of insulin-degrading enzyme (Insulysin). A potential target for drug development. *J. Biol. Chem.* **278**, 49789–49794.
11. Kuoroichkin, I. V. (2001). Insulin-degrading enzyme: embarking on amyloid destruction. *Trends Biochem. Sci.* **26** , 421–425.
12. Burgus, R., Ling, N., Butcher, M. & Guillemin, R. (1973). Primary structure of somatostatin, a hypothalamic peptide that inhibits the secretion of pituitary growth hormone. *Proc. Natl Acad. Sci. USA*, **70**, 684–688.
13. Reichlin, S. (1983). Somatostatin. *N. Engl. J. Med.* **309**, 1556–1563.
14. Viollet, M., Lepousez, G., Loudes, C., Videau, C., Simon, A. & Epelbaum, J. (2007). Somatostatinergic systems in brain: networks and functions. *Mol. Cell. Endocrinol.* **10**, 1016–1028.
15. Hayashi, M., Yamashita, A. & Shimizu, K. (1997). Somatostatin and brain-derived neurotrophic factor mRNA expression in the primate brain: decreased levels of mRNA during aging. *Brain Res.* **749**, 283–289.
16. Van Uden, E., Veinbergs, I., Mallory, M., Orlando, R. & Masliah, E. (1999). A novel role for receptor-associated protein in somatostatin modulation: implications for Alzheimer's disease. *Neuroscience*, **88**, 687–700.
17. Davis, K. L., Mohs, R. C., Marin, D. B., Purohit, D. P., Perl, D. P., Lantz, M. *et al.* (1999). Neuropeptide abnormalities in patients with early Alzheimer disease. *Arch. Gen. Psychiatry*, **56**, 981–987.
18. Nemeroff, C. B. (1999). The preeminent role of neuropeptide systems in the early pathophysiology of Alzheimer's disease: up with corticotrophin-releasing factor, down with acetylcholine. *Arch. Gen. Psychiatry*, **56**, 991–992.
19. Geci, C., How, J., Alturaihi, H. & Kumar, U. (2007). β amyloid increases somatostatin expression in cultured cortical neurons. *J. Neurochem.* **101** , 664–673.
20. Iwata, N., Tsubuki, S. & Takaki, T. (2000). Identification of the major Aβ1–42-degrading catabolic pathway in brain parenchyma: suppression leads to biochemical and pathological deposition. *Nat. Med.* **6**, 1146–1150.
21. Kumar, U. (2005). Expression of somatostatin receptor subtypes (SSTR1–5) in Alzheimer's disease brain: an immunohistochemical analysis. *Neuroscience*, **134**, 525–538.
22. Cervia, D. & Bagnoli, P. (2007). An update on somatostatin receptor signaling in native systems and new insights on their pathophysiology. *Pharmacol. Ther.* **116**, 322–324.
23. Saito, T., Iwata, N., Tsubuki, S., Takaki, T., Takano, J., Huang, S. M. *et al.* (2005). Somatostatin regulates brain amyloid β peptide Aβ42 through modulation of proteolytic degradation. *Nat. Med.* **11**, 434–439.
24. Iwata, N., Tsubuki, S. & Takaki, T. (2001). Metabolic regulation of brain Aβ by neprilysin. *Science*, **292**, 1550–1552.
25. Chesneau, V., Vekrellis, K., Rosner, M. R. & Selkoe, D. L. (2000). Purified recombinant insulin-degrading enzyme degrades amyloid β-protein but does not promote its oligomerization. *Biochem. J.* **351**, 509–516.
26. Dahms, P. & Mentlein, R. (1992). Purification of the main somatostatin-degrading proteases from rat and pig brains, their action on other neuropeptides, and their identification as endopeptidases 24.15 and 24.16. *Eur. J. Biochem.* **208**, 145–154.
27. Lucius, R. & Mentlein, R. (1991). Degradation of the neuropeptide somatostatin by cultivated neuronal and glial cells. *J. Biol. Chem.* **266**, 18907–18913.
28. Van Grondelle, W., Iglesias, C. L., Coll, E., Artzner, F., Paternostre, M., Lacombe, F. *et al.* (2007). Spontaneous

fibrillation of the native neuropeptide hormone Somatostatin-14. *J. Struct. Biol.* **160**, 211–223.
29. Grasso, G., Rizzarelli, E. & Spoto, G. (2007). AP-MALDI/MS complete characterization of insulin fragments produced by the interaction of IDE with bovine insulin. *J. Mass Spectrom.* **42**, 1590–1598.
30. Honjo, E., Watanabe, K. & Tsukamoto, T. (2002). Real-time kinetic analyses of the interaction of ricin toxin A-chain with ribosomes prove a conformational change involved in complex formation. *J. Biochem.* **131**, 267–275.
31. Yowler, B. C. & Schengrund, C. L. (2004). Botulinum neurotoxin A changes conformation upon binding to ganglioside GT1b. *Biochemistry*, **43**, 9725–9731.
32. Qiu, W. Q., Walsh, D. M., Ye, Z., Vekrellis, K., Zhang, J., Podlisny, M. B. *et al.* (1998). Insulin-degrading enzyme regulates extracellular levels of amyloid β-protein by degradation. *J. Biol. Chem.* **273**, 32730–32738.
33. Mukherjee, A., Song, E.-S., Kihiko-Ehmann, M., Goodman, J. P., Jr, Pyrek, J. S., Estus, S. & Hersh, L. B. (2000). Insulysin hydrolyzes amyloid β peptides to products that are neither neurotoxic nor deposit on amyloid plaques. *J. Neurosci.* **20**, 8745–8749.
34. Farris, W., Mansourian, S., Chang, Y., Lindsley, L., Eckman, E. A., Frosch, M. P. *et al.* (2003). Insulin-degrading enzyme regulates the levels of insulin, amyloid β-protein and the β-amyloid precursor protein intracellular domain *in vivo*. *Proc. Natl Acad. Sci. USA*, **100**, 4162–4167.
35. Miller, B. C., Eckman, E. A., Sambamurti, K., Dobbs, N., Chow, K. M., Eckman, C. B. *et al.* (2003). Amyloid-β peptide levels in brain are inversely correlated with insulysin activity levels *in vivo*. *Proc. Natl Acad. Sci. USA*, **100**, 6221–6226.
36. Winsky-Sommerer, R., Grouselle, D., Rougeot, C., Laurent, V., David, J. P., Delacourte, A. *et al.* (2003). The proprotein convertase PC2 is involved in the maturation of prosomatostatin to somatostatin-14 but not in the somatostatin deficit in Alzheimer's disease. *Neuroscience*, **122**, 437–447.
37. Wyman, J., Jr (1964). Linked functions and reciprocal effects in haemoglobin: a second look. *Adv. Protein Chem.* **19**, 223–286.
38. Hama, E. & Saido, T. C. (2005). Etiology of sporadic Alzheimer's disease: somatostatin, neprilysin and amyloid β peptide. *Med. Hypotheses*, **65**, 498–500.
39. Yaron, A., Carmel, A. & Katchalski-Katzir, E. (1972). Intramolecularly quenched fluorogenic substrates for hydrolytic enzymes. *Anal. Biochem.* **95**, 228–235.
40. Fields, G. B. & Noble, R. L. (1990). Solid phase peptide synthesis utilizing 9-fluorenylmethoxy-carbonil amino acids. *Int. J. Pept. Protein Res.* **35**, 161–214.
41. Leissring, M. A., Lu, A., Condron, M. M., Teplow, D. B., Stein, R. L., Farris, W. & Selkoe, D. J. (2003). Kinetics of amyloid β-protein degradation determined by novel fluorescence- and fluorescence polarization-based assays. *J. Biol. Chem.* **278**, 37314–37320.
42. Grasso, G., Fragai, M., Rizzarelli, E., Spoto, G. & Yeo, K. J. (2006). In situ AP-MALDI characterization of anchored MMPs. *J. Mass Spectrom.* **41**, 1561–1569.
43. D'Agata, R., Grasso, G., Iacono, G., Spoto, G. & Vecchio, G. (2006). Lectin recognition of a new SOD mimic bioconjugate studied with surface plasmon resonance imaging. *Org. Biomol. Chem.* **4**, 610–612.
44. Myszka, D. G., He, X., Dembo, M., Morton, T. A. & Goldstein, B. (1998). Extending the range of rate constants available from BIACORE: interpreting mass transport-influenced binding data. *Biophys. J.* **75**, 583–594.
45. Grasso, G., D'Agata, R., Rizzarelli, E., Spoto, G., D'Andrea, L., Pedone, C. *et al.* (2005). Activity of anchored human matrix metalloproteinase-1 catalytic domain on Au (111) surfaces monitored by ESI-MS. *J. Mass Spectrom.* **40**, 1565–1571.
46. Lahiri, J., Isaacs, L., Tien, J. & Whitesides, G. M. (1999). A strategy for the generation of surfaces presenting ligands for studies of binding based on an active ester as a common reactive intermediate: a surface plasmon resonance study. *Anal. Chem.* **71**, 777–790.